RSC Advances

ROYAL SOCIETY OF CHEMISTRY

www.rsc.org/advances

Journal Name

PAPER

Facile synthesis of Cu_2PO_4OH hierarchical nanostructures and the improved catalytic activity by hydroxyl group†

Received 00th January 2015,
Accepted 00th January 2015

DOI: 10.1039/x0xx00000x

www.rsc.org/

Yunxuan Zhao, [a] Fei Teng, [a*] Juan Xu, [a] Zailun Liu, [a] Yang Yang, [a] Qiqi Zhang, [a] Wenqing Yao [b]

One- and three-dimensional (1D, 3D) Cu_2PO_4OH hierarchical architectures have been successfully prepared by a facile hydrothermal method, mainly through adjusting the precursors concentrations. A possible splitting mechanism is proposed to understand the evolution from 1D to 3D hierarchical architectures. Besides, through experiments and density functional theory (DFT) calculations, we find that copper hydroxyphosphate (Cu_2PO_4OH) shows an excellent catalytic activity for the degradation of rhodamine B (RhB). This has been mainly ascribed to the contribution of hydroxyl groups contained in Cu_2PO_4OH, which favours to form more hydroxyl radicals. Moreover, both partial density of states (PDOS) and total density of states (TDOS) have confirmed that conduction band (CB) is affected by part of O 2p orbitals of hydroxyls; thus the hydroxyl group is responsible for the increased band gap and the positive VB of Cu_2PO_4OH. This study suggests that the new photocatalysts or photoelectric materials can be developed through introducing hydroxyl groups.

Introduction

To date, various nanostructures from one-dimensional (1D) to three-dimensional (3D) have been intensively studied due to their excellent properties, such as catalysis, [1] gas sensors, [2] optoelectronics, [3] battery electrodes, [4] and so on. Nowadays, incredible efforts have been devoted to develop new methods to fabricate nanomaterials with new hierarchical architectures. [5-6] Among these, metal phosphates have attracted considerable attention due to various applications in catalysis, chemical materials and intercalation chemistry. [7-8] Recently, copper hydroxyphosphate [9] have attracted significant attention due to its excellent catalytic properties for hydroxylation of phenol, [10] oxidation of azo dyes [11] and epoxidation of styrene. [12] It is well known that the particle morphology has a significant influence on the physicochemical properties of materials. [9,13] Nevertheless, it still remains a big challenge to develop a facile, environment-friendly method without using any templates or surfactants for the preparation of novel micro/nanostructures. In particular, some of hydroxyl-containing photocatalysts have been developed, *e. g.*, $Bi_2O_2[BO_2(OH)]$, [14] $Bi_2O(OH)_2SO_4$, [15] MnOOH,[16] *etc*. However, the role of hydroxyl contained in the material in the photo oxidation activity has not been well understood and revealed.

Herein, without using any templates or surfactants, Cu_2PO_4OH hierarchical architectures were prepared by a simple hydrothermal method. A crystal splitting mechanism was proposed to understand the formation of 1D to 3D hierarchical architectures. The photo degradation of RhB under ultraviolet (UV)-light irradiation (≤420nm) was used as the probing reaction to explore the catalytic activities of the samples. Besides, the contrast experiments, in which dimethyl sulfoxide (DMSO) was used as the scavenger of hydroxyl radicals (•OH) and ammonium oxalate ($(NH_4)_2C_2O_4$) as the electron scavenger, confirmed that the hydroxyl group contained in Cu_2PO_4OH favoured the generation of more •OH free radicals. We also investigated the influence of inorganic ions on the degradation of RhB. It showed that Cu^{2+} and PO_4^{3-} ions have significantly reduced the degradation rate. Furthermore, the structure-property relationship was also studied through DFT calculations. It suggests that the hydroxyl groups contained in Cu_2PO_4OH greatly affect electronic structure and contribute the CB of Cu_2PO_4OH, leading to a wide band gap. The regulation strategy of hydroxyl groups would provide us a novel idea to develop new, excellent photocatalysts or photoelectric materials.

Experimental

Preparation of Strawsheaf-like (S) Cu_2PO_4OH

In a typical synthesis, 2.57 mmol of KH_2PO_4 was added into 60 ml of 0.083 M $CuCl_2 \cdot 2H_2O$ (5 mmol) solution under constant magnetic stirring. Then, 2.57 mmol of KOH was added into the solution. After stirring for 10 minutes, the mixture was transferred to a Teflon-lined stainless steel autoclave and maintained at 140 °C for 24 h. After the autoclave was cooled to room temperature naturally, the light green product was obtained by centrifugation, washed with deionized water for several times, and dried at 60 °C for 6 h.

Preparation of Dumbbell- (D) and Butterfly-like (B) Cu_2PO_4OH

The similar procedures as above were employed to prepare dumbbell-like (D) and butterfly-like (B) Cu_2PO_4OH samples, while the precursors concentrations were all reduced to 40% and 8% as high as those for the preparation of strawsheaf-like

[a]. *Jiangsu Engineering and Technology Research Centre of Environmental Cleaning Materials (ECM), Jiangsu Key Laboratory of Atmospheric Environment Monitoring and Pollution Control (AEMPC), Jiangsu Joint Laboratory of Atmospheric Pollution Control (APC), Collaborative Innovation Center of Atmospheric Environment and Equipment Technology (AEET), School of Environmental Science and Engineering, Nanjing University of Information Science & Technology, 219 Ningliu Road, Nanjing 210044, China;*
[b]*Department of Chemistry, Tsinghua University, Beijing 100084, China.*
Electronic Supplementary Information (ESI) available: [details of any supplementary information available should be included here]. See DOI: 10.1039/x0xx00000x

sample, respectively. In order to describe clearly, we used the copper ion concentration to represent the precursors concentrations.

Preparation of CuO flowers and Cu

Synthesis of CuO flowers. 20 ml of 0.5M NaOH aqueous solution was directly added into 20 ml of $CuSO_4$ (7.8 mmol) solution, and a blue $Cu(OH)_2$ precipitate formed immediately. Subsequently, hexamethylenetetramine (HMTA) (50mmol) was added to the above mixture under continuous stirring at room temperature. After being stirring for 10 minutes, the above mixture was transferred into a 60 ml Teflon-lined stainless steel autoclave and maintained at 120 °C for 24h. When the reaction was completed, the autoclave was cooled to room temperature naturally. The product was harvested by centrifugation, washed with deionized water several times, and then dried in air at 60 °C for 6h.

Synthesis of Cu: 0.01 mol ethylenediaminetetraacetic acid disodium salt (EDTA-2Na), cupric sulfate, HMTA were added into 35 ml deionized water in sequence under stirring at room temperature. After 30 min, 0.8 g cetyltrimethyl ammonium bromide was added into the aqueous system and kept stirring for another 30 min to form a clear solution. The solution was then transferred to a 50-ml Teflon-lined stainless-steel autoclave and heated at 180 °C for 48 h. After the autoclave was cooled to room temperature naturally, the solid was collected by centrifugation, washed with ethanol and deionized water for 3 times, respectively. Finally, the product was dried at 60 °C overnight.

Characterization

The crystal structures of the samples were determined by X-ray powder polycrystalline diffractometer (Rigaku D/max-2550VB), using graphite monochromatized Cu Kα radiation (λ= 0.154 nm), operating at 40 kV and 50mA. The XRD patterns were obtained in the range of 20-80° (2θ) at a scanning rate of 7° min^{-1}. The samples were characterized on a scanning electron microscope (SEM, Hitachi SU-1510) with an acceleration voltage of 15 keV. UV-vis diffused reflectance spectra of the samples were obtained using a UV-vis spectrophotometer (UV-2550, Shimadzu, Japan). $BaSO_4$ was used as a reflectance standard in a UV-vis diffuse reflectance experiment. Fourier transform infrared spectra (FT-IR) were recorded on a Fourier transform infrared spectrometer (FT-IR, KBr disk method; Thermo Scientific Nicolet iS5) at wavenumbers 400-4000 cm^{-1}. Nitrogen sorption isotherms were performed at 77 K and < 10^{-4} bar on a Micromeritics ASAP2010 gas adsorption analyzer. Each sample was degassed at 90 °C for 5 h before measurements. Nitrogen adsorption–desorption isotherms were obtained at 77 K using the Autosorb-iQ physicoadsorption apparatus (Quantachrome). Surface area was calculated by the Brunauer-Emmett-Teller (BET) method.

Catalytic activity measurements

The catalytic activity of the sample was performed under UV light irradiation (λ≤420 nm). 0.1 g of catalyst and 2 μl of H_2O_2 (30 vol.%) were dispersed in 200 mL of 10 mg/L RhB aqueous solution, which was irradiated with a 500-W high pressure Xe lamp as light source. The reaction system was placed in a sealed black box with the top opened, and the distance between the reaction system and light source was 15 cm. Before the lamp was turned on, the suspension was continuously stirred for 10 min in the dark to ensure the establishment of an adsorption–desorption equilibrium between the catalyst and RhB. During degradation, 3 mL of the solution was collected using a pipette at intervals of irradiation, and subsequently centrifuged to remove the catalyst. UV-vis spectra were recorded using a Spectrumlab 722sp spectrophotometer to determine the concentration of RhB.

Theoretical calculations

The energy band structure, total and partial densities of states (TDOS, PDOS) were calculated by density functional theory (DFT) as implemented in the CASTEP software. The calculations were carried out using the generalized gradient approximation (GGA) level and Perdew-Burke-Ernzerh (PBE) formalism for combination of exchange and correlation function. The cut-off energy is chosen as 400 eV, and a density of (3×3×4) Monkhorst-Pack *K*-point was adopted to sample the Brillouin zone.

Results and discussion

Effect of precursor concentration on the samples

Fig. 1 shows the XRD patterns of the S, D and B-Cu_2PO_4OH samples, which were prepared at different precursors concentrations. It is obvious that all the diffraction peaks can be well indexed to the standard card (JCPDS 72-0462). No impurity peaks can be detected, confirming the formation of phase-pure Cu_2PO_4OH at different precursor solution concentrations.

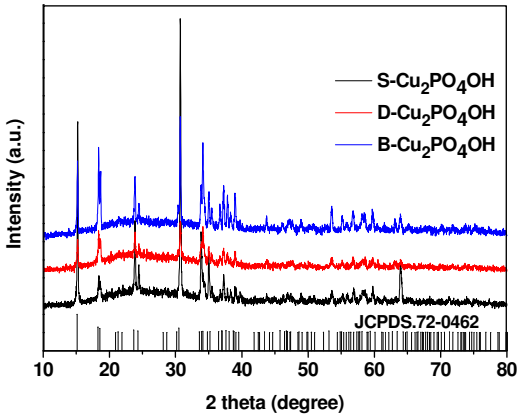

Fig. 1 X-ray diffraction patterns (XRD) of the samples synthesized at different precursors concentrations: S-Cu_2PO_4OH (0.083 M); D-Cu_2PO_4OH (0.033 M); B- Cu_2PO_4OH (0.007 M).

Table 1 BET areas and morphologies of the samples prepared at different precursors concentrations.

Samples	Precursors concentrations	[a] Surface area (m^2/g)	Morphology
S-Cu_2PO_4OH	0.083M	1.0	Straw sheaves
D-Cu_2PO_4OH	0.033M	5.3	Dumbbells
B-Cu_2PO_4OH	0.007M	16.1	Butterflies

[a] Surface area, calculated by the Brunauer-Emmett-Teller (BET) method;

Journal Name PAPER

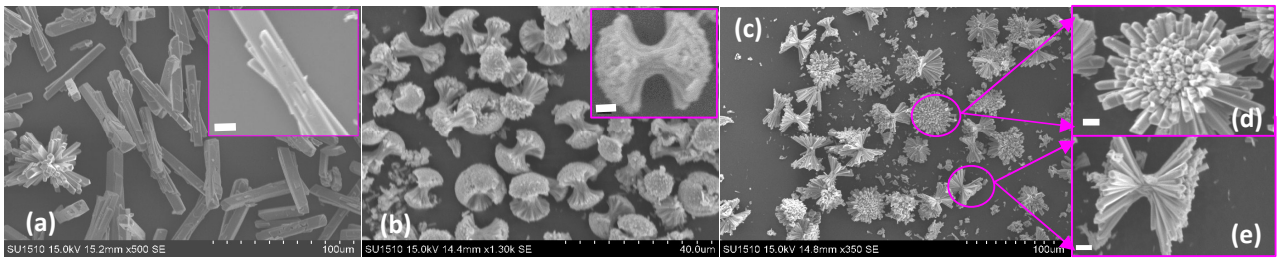

Fig. 2 Scanning electron microscopy (SEM) images of the samples synthesized at different precursors concentrations: (a) 0.083M; (b) 0.033M; (c) 0.007M; (c, d) B-Cu_2PO_4OH observed along different directions; Scale bar = 5 µm.

As observed from Fig. 2, the Cu_2PO_4OH samples show significantly different hierarchical architectures, namely, strawsheaves (Fig. 2a), dumbbells (Fig. 2b) and butterflies (Fig. 2c). At a high concentration (0.083 M), Fig. 2a reveals that the individual straw sheaf has a size of 60 µm × 8 µm, and a feeble splitting occurs in the central section of microrod (the inset of Fig. 2a). At a low concentration (0.033 M), the well-defined, uniform dumbbells form with the diameters of 13-17 µm (Fig. 2b), and the dumbbell consists of microrods. While further reducing the precursors concentrations (0.007 M), the butterfly-like superstructures have formed, which consists of the microrods about 27-35 µm in diameters (Fig. 2c). Further viewed along the axial direction (Fig. 2d), the fantail–like structure consists of a large number of microrods with the diameters of 35-45 µm. Fig. 2e reveals that an obvious splitting occurs for the superstructures, which leads to a large BET area of 16.1 m^2/g. It is obvious that the precursors concentrations have a significant influence on the morphology and size of the sample (Table 1).

Effects of reaction time and temperature on the samples

To understand the formation process of the Cu_2PO_4OH straw sheaves, the time and temperature-dependent experiments were carried out, while keeping the other experimental conditions constant. Fig. S1 (seeing electronic supporting information (ESI)) shows the XRD patterns of the samples prepared at different reaction times and temperatures. All the diffraction peaks of the as-obtained samples can be indexed as orthorhombic structure (JCPDS No. 72-0462).

Furthermore, the (220) peak becomes sharp and narrow with increasing reaction time and temperatures, suggesting that average crystallite size increases (Fig. S2(a,b)). Herein, Scherrer's Equation is used to calculate the average crystal size.

$$D=K\lambda/(B\cos\theta) \quad (1)$$

where D is the mean diameter of crystallites, K is taken as 0.89, and λ is the wavelength of X-ray (where Cu K_α =0.154178 nm), B is the full width of diffraction peak at half of the maximum intensity, and θ is Bragg angle. The results are displayed in Fig. S2(c,d). The average sizes of crystallites increase from 34.7 nm to 118.9 nm. It is obvious that the crystals grow larger with increasing reaction time or temperatures of crystallites increase from 34.7 nm to 118.9 nm. A high temperature or a long time is beneficial to crystal growth.

As observed from Fig. S 3a (seeing ESI), only Cu_2PO_4OH microrods form at the initial stage (12 h). With increasing the reaction time, the strawsheaf-like Cu_2PO_4OH sample form (Fig. S3 (b-d) of ESI), and the crystallinity and size of the sample also increase (Fig. S 1a and S 2c of ESI). In comparison, the Cu_2PO_4OH sample prepared at 24 h exhibits high peaks intensities, which means a high crystallinity.[17] Fig. S4 shows the SEM images of the samples prepared at different temperatures (80-180 °C). It seems that reaction temperature has little influence on the morphology of the sample in our study.

Growth mechanism of Cu_2PO_4OH

On the basis of the above experimental results, a possible splitting mechanism is proposed to explain the formation of hierarchical architectures, which has been proposed for the other materials. [18-23] It has been reported[19] that crystal splitting is associated with crystal growth rate, which is strongly dependent on the supersaturation of solution. Since Cu_2PO_4OH was synthesized without using any templates or surfactants, we are reasonable to assume that the splitting growth of crystal would be due to the variation in concentrations of raw reagents [24]. Herein, the growth process of crystals could be proposed as follows: at the initial stage, the $Cu(OH)_2$ nanocrystals would form through the reaction between Cu^{2+} and OH^-. With increasing reaction time or temperature, the $Cu(OH)_2$ nanoparticles would form. Subsequently, the transformation from $Cu(OH)_2$ to Cu_2PO_4OH would occur, which is driven kinetically and thermodynamically. [25] In our synthesis, the chemical reactions (2, 3) are proposed as follows:

$$Cu^{2+} + 2OH^- \rightarrow Cu(OH)_2 \quad (2)$$

$$Cu^{2+} + Cu(OH)_2 + H_2PO_4^- \rightarrow Cu_2PO_4OH + 2H_2O + H^+ \quad (3)$$

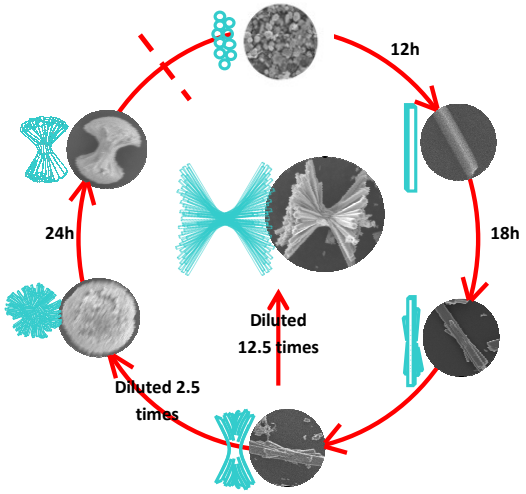

Scheme 1 Schematic diagram for the morphological evolution and growth of Cu_2PO_4OH.

In particular, the crystal splitting growth has been discovered previously in the other crystals, such as Bi_2S_3, [19] Ce(1,3,5-BTC)$(H_2O)_6$, [20] CuO, [26] and so on. It has been reported [27] that crystal

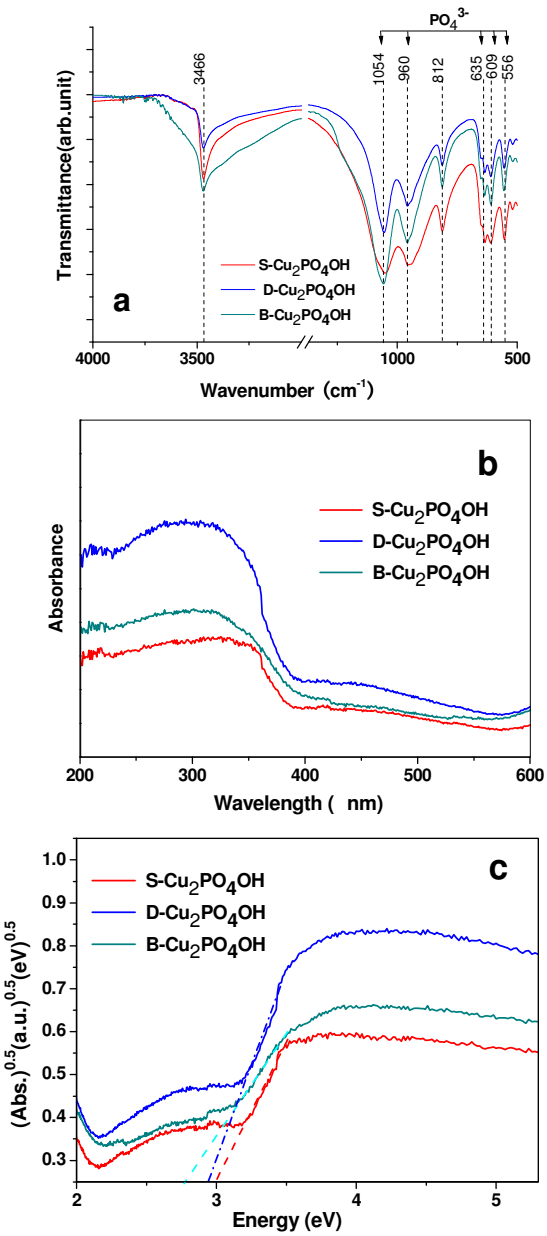

Fig. 3 FTIR (a) and UV–visible diffuse reflectance spectra (UV-DRS) (b) and Tauc plots (c) of the Cu_2PO_4OH samples.

splitting is closely relative to the fast growth rate that is dependent on the oversaturation. In our preparation, the splitting of Cu_2PO_4OH may be mainly caused by the precursors concentrations. On base of the morphology evolution from butterfly to microsphere, we can observe that the extent of crystal splitting decreases, while the concentration of Cu(II) ion increases from 0.007 to 0.033 M. The morphology of Cu_2PO_4OH evolves from sphere to dumbbell with increasing reaction time or temperature. These results are consistent with previous studies, [20,26] namely, the splitting degree decreases as the precursors concentrations increases. It is reported that the crystal splitting is possible if the oversaturation exceeds at a certain "critical" level. [27] At a higher concentration, however, more nuclei

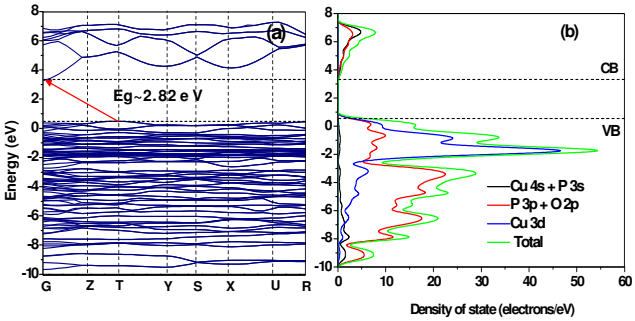

Fig. 4 (a) Band structure and (b) total and partial density of state (DOS) of Cu_2PO_4OH calculated by DFT.

will form and the crystal growth rate becomes slower, [19] which will prohibit the splitting growth process. The schematic morphology evolution diagram of Cu_2PO_4OH is presented in Scheme 1.

Effect of hydroxyl on energy band and electronic structure of Cu_2PO_4OH

To further detect the presence of hydroxyl, the FTIR spectra of Cu_2PO_4OH samples were conducted (Fig. 3a). The FTIR spectra of the samples are approximately identical after deducting background. It is noteworthy that the absorption bands at 3466 and 812 cm^{-1} correspond to the lattice vibration modes of hydroxyl, and the vibration mode of phosphate is found at 1054, 960, 635, 609 and 556 cm^{-1}.[9] The results demonstrate that the samples contain hydroxyl and phosphate.

Besides, the electronic structure of Cu_2PO_4OH was calculated by the *ab* initio density functional theory (DFT) using the CASTEP program package (Fig. 4). Valence band maximum (VBM) at the T point and conduction band minimum (CBM) at the G point confirmed the indirect band gap property of Cu_2PO_4OH (Fig. 4(a)). It can be found that the band gap between VBM and CBM is 2.82 eV, which is close to experimental results (2.77-3.0 eV) by UV-DRS measurement (Fig. 3b, c). The calculated result agrees well with a common feature of DFT calculations. [15,28] At the same time, an obvious dispersed energy can be observed, which would favour for the transportation of photo-generated electrons and holes,[29] thus improving the photocatalytic activity. Moreover, the total density of states (TDOS) and the partial density of states (PDOS) are presented in Fig. 4(b). It can be seen that VB is mainly composed of Cu 4s and P 3p orbits, while the CB bottom is mainly composed of Cu 3d, O 2p and P 3p orbits. For Cu_2PO_4OH, the photogenrated charge transfer would occur from the hybridization orbits of both Cu 4s and P 3p to the empty Cu 3d orbit.

In order to further understand the effect of hydroxyl on the energy band structure of Cu_2PO_4OH, we have calculated another optimized super cell, in which the hydroxyls were removed (Fig. 5(a, b)). Compared with Cu_2PO_4OH, the distance between $O_{(3)}$ and $Cu_{(2)}$ of the optimized super cell increases from 2.121 to 2.937 Å and the bond angles of $P_{(1)}$-$O_{(3)}$-$Cu_{(2)}$ and $O_{(3)}$-$Cu_{(2)}$-$O_{(2)}$ change from 138.710° and 91.909° to 79.670° and 134.862°, respectively, indicating that hydroxyl can greatly affect the crystal structure. Moreover, when the hydroxyls are removed, its energy band gap has changed from an indirect band gap to a direct band gap, and the band gap has decreased from 2.82 eV to 1.6 eV (Fig. 5(e)). In fact, the VB of the optimized cell without hydroxyl is similar to the original Cu_2PO_4OH cell, but its CBM decreases from 3.3 eV to 2.0 eV (Fig. 5 (c, d)). The results are similar to the previous DFT calculations of $Bi_4B_2O_9$ and $Bi_2O_2[BO_2(OH)]$. [14] It suggests that the P 3p and O 2p (result from OH^-) contribute to CB bottom. To conclude, the hydroxyl groups can affect electronic structure and contribute to the CB of Cu_2PO_4OH.

Journal Name PAPER

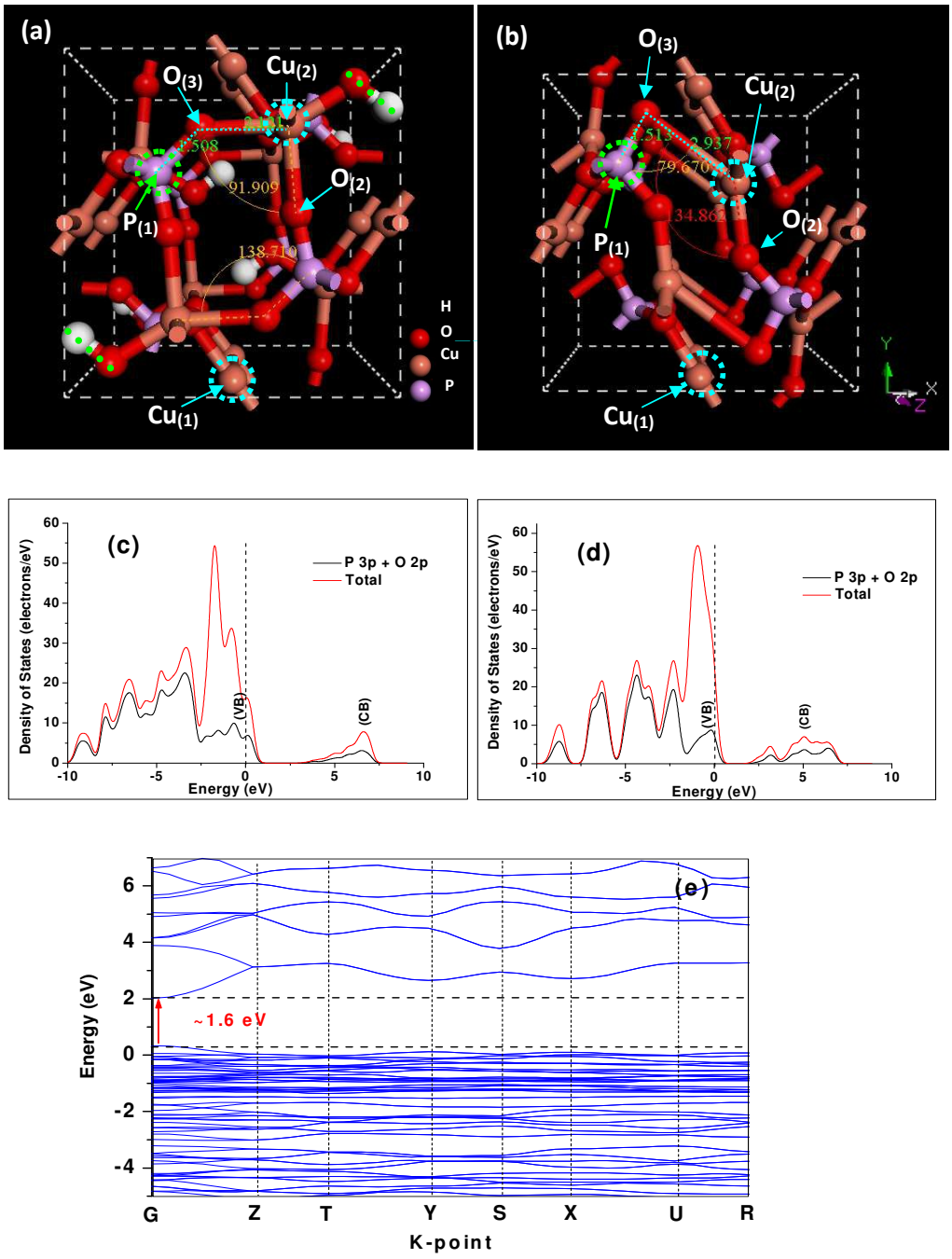

Fig. 5 Crystal structures (a) and TDOS and PDOS (c) of Cu_2PO_4OH ; Crystal structures (b), TDOS and PDOS (d) and band structure (e) of optimized super cell without hydroxyl group.

Effect of hydroxyl on catalytic activity of Cu_2PO_4OH

The effect of the amount of catalyst in reaction was investigated in Fig. S5. It can be obviously seen that the degradation efficiency was low with only 61.1% after 40 minutes. When adding 0.015g S-Cu_2PO_4OH in reaction, the degradation efficiency reaches at 75.7% after 40 minutes, indicating the S-Cu_2PO_4OH t is active. When the amount of the S-Cu_2PO_4OH is increased to 0.05, 0.1 and 0.15g, the degradation efficiency reaches 85.4, 94.7 and 83.5%, respectively. It is well-known that more S-Cu2PO4OH catalyst in solution will lead to the solution more turbid, which will interfered the penetration of light transmission and weaken the light absorption, then influence the catalytic degradation efficiency. Fig S 6a shows the degradation curves of RhB over the Cu_2PO_4OH samples in the presence of H_2O_2 under UV light irradiation. The S-Cu_2PO_4OH sample exhibits a higher catalytic activity than the others. In Fig S

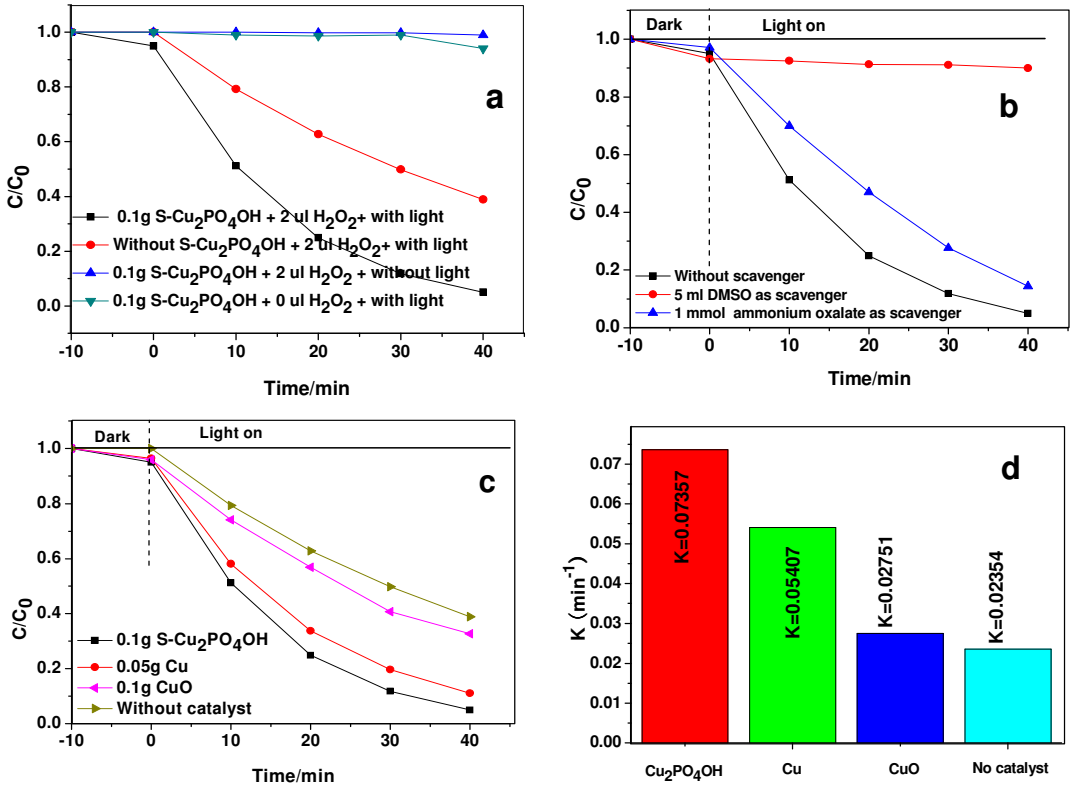

Fig. 6 (a) Degradation curves of RhB at different test conditions; (b) Effect of different scavengers on the degradation activity of RhB over Cu_2PO_4OH under UV irradiation; (c) Degradation curves and (d) apparent reaction kinetic constants of the samples for the degradation of rhodamine B (RhB) under UV irradiation ($\lambda \leq 420$ nm).

6b, the apparent reaction rate constant (k_a) of S-Cu_2PO_4OH (0.074 min^{-1}) is higher than D-Cu_2PO_4OH (0.055 min^{-1}) and B-Cu_2PO_4OH (0.051 min^{-1}). In order to understand their different activities, the crystallinities, absorbances and BET areas of the samples are investigated. Although the B-Cu_2PO_4OH sample has a higher BET area (16.1 m^2g^{-1}) (Table 1) and a higher absorbance ((Fig. 3a), its crystallinity is lower (39.8%) than D-Cu_2PO_4OH (5.3 m^2g^{-1}, 48.2%) and S-Cu_2PO_4OH (1.0 m^2g^{-1}, 55.9%). It seems that the BET area and absorbance are not the predominated factor for the activity in this study. The low crystallinity suggests that more defects are contained in crystal. [17] It is reported that the bulk defects of photocatalysts are usually considered to be the recombination centres for electrons and holes, [17] resulting in a low photocatalytic activity. Therefore, the S-Cu_2PO_4OH shows higher catalytic activities could be attributed to their high crystallinities. The stability of catalyst has been discussed, as shown in Fig. S7. It is noteworthy that its degradation efficiency is scarcely reduced after five cycles, indicating a good stability of Cu2PO4OH catalyst. Fig. S8 shows the total organic carbon (TOC) value of the irradiated solution is analyzed to evaluate the degradation of RhB. It can be observed that during the degradation of RhB dye, the value declines with the time, with a velue of 33% after 40 minutes. It does not reach a complete conversion to CO2 and H2O. It may be that the dye has been decomposed into the other small molecules and needs more time to complete degradation. Herein, we can not determine the intermediates, due to our limited experimental conditions.

Furthermore, the comparative tests have been carried out to investigate the catalytic activity of S-Cu_2PO_4OH for degradation of RhB when using 2 μl of H_2O_2 (Fig. 6a). After 40 min irradiation, 95% of RhB can be degraded by S-Cu_2PO_4OH; but only 61% of RhB can be degraded without catalyst, demonstrating that Cu_2PO_4OH contributes the improvement of degradation activity. Besides, without UV irradiation or H_2O_2 in the presence of S-Cu_2PO_4OH catalyst, RhB can not be degraded. Overall, the comparative experiments suggest that the presences of S-Cu_2PO_4OH catalyst and UV irradiation and H_2O_2 are necessary for the degradation of RhB.

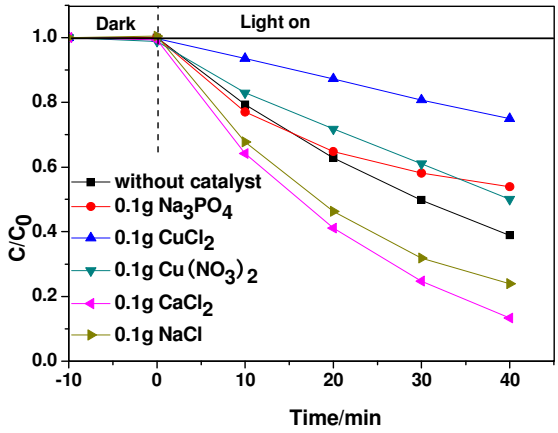

Fig. 7 Degradation curves of RhB while adding different inorganic salts.

In addition, the trapping experiments have also been performed to explore the photocatalytic degradation process, in which ammonium oxalate and dimethylsulfoxide (DMSO) are used as the hole scavenger [30] and the hydroxyl radical scavenger, [31] respectively (Fig. 6b). When adding 1 mmol ammonium oxalate, the degradation activity of RhB decreases slightly; but the degradation reaction has been nearly inhibited when adding 5 mL DMSO. The results indicate that the hydroxyl radicals could be the major active oxidative species for RhB over S-Cu_2PO_4OH.

Moreover, to further understand the role of hydroxyl in S-Cu_2PO_4OH in the degradation reaction, we have compared the degradation activities of RhB while using different copper-containing catalysts (Fig. 6c). It is found that Cu, CuO and Cu_2PO_4OH are catalytically active. In Fig. 6d, the apparent reaction kinetic rate constant (k_a) over Cu_2PO_4OH is determined to be 0.07357 min^{-1}, which is higher than those of the others. Cu_2PO_4OH exhibits a higher catalytic activity than Cu and CuO.

To reveal the role of inorganic ion in the degradation reaction, the comparative tests have been investigated (Fig 7). Compared with $CuCl_2$, $CaCl_2$ has improved activity greatly, whereas $CuCl_2$ has refrains the reaction greatly, suggesting that the Cu^{2+} ion can refrain the degradation reaction. We hold that Cu^{2+} ion possesses the vacancy 3d orbit, thus a coordination bond could form between Cu^{2+} and H_2O_2. The coordination bond may inhibit the decomposition of H_2O_2, i.e. refraining the generation of hydroxyl radicals. The positive Ca^{2+} may promote the decomposition of H_2O_2. Similarly, NaCl also promotes the reaction, but Na^+ is also less active than Ca^{2+} slightly, which may be closely relative to their different radii and charges. The higher charge Ca^{2+} ions have stronger polarization effect than Na^+, which may favours the activation of H_2O_2. This would be beneficial to the decomposition of H_2O_2. It should be pointed out that the real reason is still unclear. Compared NaCl with Na_3PO_4, Na_3PO_4 has greatly inhibited the degradation reaction, which may be relative to their different pH values. It seems that a high pH value does not favour the reaction; [31] Nevertheless, compared $CuCl_2$ with $Cu(NO_3)_2$, the Cl^- ions also have an inhibitory effect on the degradation RhB more than NO_3^-. Herein, the real reasons for different degradation activities are still unclear, which needs further studying.

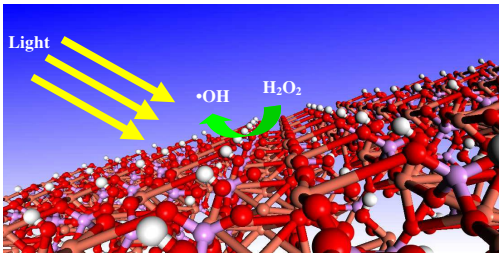

Fig. 8 The mechanism for formation of hydroxyl radicals.

The activity difference between Cu_2PO_4OH and $Cu_4O(PO_4)_2$ may be relative to the crystal structure. As reported in previous studies, [32] Cu_2PO_4OH has an orthorhombic space group (*Pnnm*) with the unit cell parameters of *a*=8.062 Å, *b*=8.384 Å, and *c*=5.881 Å. It consists of PO_4 tetrahedron, $Cu(2)O_5$ trigonal bipyramid, $Cu(1)O_6$ octahedron and OH group. In our study, nevertheless, Cu_2PO_4OH crystallizes in an orthorhombic structure with space group *Pnnm* and lattice constants *a*=8.11 Å, *b*=8.47 Å, and *c*=5.92 Å. [33] It is obvious that the OH group attaches on copper sites of Cu_2PO_4OH. In comparison, $Cu_4O(PO_4)_2$ results from dehydration of Cu_2PO_4OH. This is only their structure difference. [32] Herein, we could hold that the hydroxyl of Cu_2PO_4OH may favour to improve catalytic properties. Xiao et al. have also confirmed that Cu_2PO_4OH also shows a higher catalytic activity than $Cu_4O(PO_4)_2$ in the hydroxylation of phenol by hydrogen peroxide. [34]

On base of the discussion above, we hold that the catalytic degradation of RhB dye over Cu_2PO_4OH is affected by two main factors as follows: (i) the separation and transfer efficiencies of photogenerated electrons and holes; (ii) the number of the formed •OH radicals. First, due to the presence of hydroxyl groups, Cu_2PO_4OH has a more positive E_{VB} (3.38 eV) (Table S1) than that (2.7 eV) ofTiO_2, which is higher than E^o ($\cdot OH/OH^-$)=2.38 eV. This would favour to react with H_2O and/or H_2O_2 to produce more •OH radicals. As a result, the more •OH radicals and/or highly positive holes favour for the degradation reaction. Second, it has been reported [35-36] that the hydroxyl groups in crystal structure are easy to form hydroxyl radicals under light excitation. In particular, Xiao et al. [34] have proposed a tentative mechanism for the formation of •OH, leading to an enhanced catalytic performance. Herein, the chemical reactions (4) may occur as follows in our reaction system:

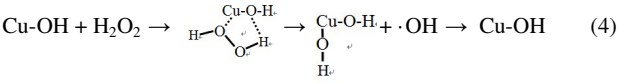

Under light irradiation, the interaction of Cu-OH with H_2O_2, i.e. a coordinate bond and a hydrogen bond, would facilitate the formation of ·OH, which could attribute to the high catalytic activity (Fig. 7).

Conclusions

To conclude, novel Cu_2PO_4OH hierarchical architectures can be prepared by a facile hydrothermal method. The Cu_2PO_4OH exhibits an excellent activity for the degradation of RhB, which has been mainly attributed to the hydroxyl groups in Cu_2PO_4OH. Both PODS and TDOS results demonstrate that the hydroxyl group is responsible for the increased band gap and positive VB of Cu_2PO_4OH. This study suggests that the new photocatalysts or photoelectric materials can be developed through introducing hydroxyl groups.

Acknowledgements

This work is financially supported by National Science Foundation of China (21377060), the Project Funded by the Science and Technology Infrastructure Program of Jiangsu (BM2013139), Jiangsu Science Foundation of China (BK2012862), Six Talent Climax Foundation of Jiangsu (20100292), Jiangsu Province of Academic Scientific Research Industrialization Projects (JHB2012-10), the Key Project of Environmental Protection Program of Jiangsu (20130005), A Project Funded by the Priority Academic Program Development of Jiangsu Higher Education Institutions (PAPD) sponsored by SRF for ROCS, SEM (2013S002), "333" Outstanding Youth Scientist Foundation of Jiangsu (2011015).

Notes and references

Corresponding author. tfwd@163.com (F.Teng); phone/fax: 86-25-58731090

1. G. R. Patzke, F. Krumeich and R. Nesper, *Angew. Chem. Int. Ed.*, 2002, **41**, 2446-2461.
2. F. Favier, E. C. Walter, M. P. Zach, T. Benter and R. M. Penner, *Science.*, 2001, **293**, 2227-2231.
3. X. Duan, Y. Huang, Y. Cui, J. Wang and C. M. Lieber, *Nature.*, 2001, **409**, 66-69.
4. A. M. Cao, J. S. Hu, H. P. Liang and L. J. Wan, *Angew. Chem.*

Int. Ed., 2005, **44**, 4391-4395.
5. L. Kang, Z. Wang, Z. Cao, Y. Ma, H. Fu and J. Yao, *J. Am. Chem. Soc.*, 2007, **129**, 7305-7312.
6. Z. Sun, J. H. Kim, Y. Zhao, F. Bijarbooneh, V. Malgras, Y. Lee, Y.-M. Kang and S. X. Dou, *J. Am. Chem. Soc.*, 2011, **133**, 19314-19317.
7. C. Pan and Y. Zhu, *Environ. Sci. Technol.*, 2010, **44**, 5570-5574.
8. Z. Yi, J. Ye, N. Kikugawa, T. Kako, S. Ouyang, H. Stuart-Williams, H. Yang, J. Cao, W. Luo and Z. Li, *Nat. Mater.*, 2010, **9**, 559-564.
9. I. S. Cho, D. W. Kim, S. Lee, C. H. Kwak, S. T. Bae, J. H. Noh, S. H. Yoon, H. S. Jung, D. W. Kim and K. S. Hong, *Adv. Funct. Mater.*, 2008, **18**, 2154-2162.
10. F.-S. Xiao, J. Sun, X. Meng, R. Yu, H. Yuan, D. Jiang, S. Qiu and R. Xu, *Appl. Catal. A.*, 2001, **207**, 267-271.
11. Y. Zhan, H. Li and Y. Chen, *J. Hazard. Mater.*, 2010, **180**, 481-485.
12. X. Meng, K. Lin, J. Sun, M. Yang, D. Jiang and F.-S. Xiao, *Catal. Lett.*, 2001, **71**, 241-244.
13. J. Xu and D. Xue, *J. Phys. Chem. B.*, 2006, **110**, 7750-7756.
14. H. Huang, Y. He, Z. Lin, L. Kang and Y. Zhang, *J. Phys. Chem. C.*, 2013, **117**, 22986-22994.
15. H. Tian, F. Teng, J. Xu, S. Lou, N. Li, Y. Zhao and M. Chen, *Sci. Rep-UK.*, 2015, **5**.
16. H. Liu, Y. Jin, N. Li, L. Wang, S. Lou, P. Sun, X. Hua, K. Wang, F. Teng and M. Chen, *Nano.*, 2014, **9**.
17. B. Ohtani, *J. Photochem. Photobiol.C.*, 2010, **11**, 157-178.
18. K. Liu, H. You, G. Jia, Y. Zheng, Y. Huang, Y. Song, M. Yang, L. Zhang and H. Zhang, *Cryst. Growth & Des.*, 2009, **10**, 790-797.
19. J. Tang and A. P. Alivisatos, *Nano Lett.*, 2006, **6**, 2701-2706.
20. K. Liu, Y. Zheng, G. Jia, M. Yang, Y. Song, N. Guo and H. You, *J. Solid State Chem.*, 2010, **183**, 2309-2316.
21. C. Lu, L. Qi, J. Yang, X. Wang, D. Zhang, J. Xie and J. Ma, *Adv. Mater.*, 2005, **17**, 2562-2567..
22. H. Zhang, C. Shen, S. Chen, Z. Xu, F. Liu, J. Li and H. Gao, *Nanotechnology.*, 2005, **16**, 267.
23. J. Yang, F. C. Meldrum and J. H. Fendler, *J.Phys. Chem.*, 1995, **99**, 5500-5504.
24. D. Chen and J. Ye, *Chem. Mater.*, 2007, **19**, 4585-4591.
25. J.W. Mullin. Crystallization, 3rd ed.; Butterworth-Heinemaan: Oxford, 1997.
26. Y. Zhao, H. Shi, M. Chen and F. Teng, *CrystEngComm.,* 2014, **16**, 2417-2423.
27. P. Punin and O. Yu, Crystal Splitting. Zap. Vses. Mineral. Ova., part 110, No. 6, 666–686 (Russian).
28. C. Feng, F. Teng, Z. Liu, C. Chang, Y. Zhao, S. Wang, M. Chen, W. Yao and Y. Zhu, *J. Mol. Catal. A: Chem.*, 2015, **401**, 35-40.
29. W. Wei, Y. Dai and B. Huang, *J. Phys. Chem. C.*, 2009, **113**, 5658-5663.
30. Y. Zhang, N. Zhang, Z.-R. Tang and Y.-J. Xu, *Chem. Sci.*, 2013, **4**, 1820-1824.
31. K. Wang, J. Xu, X. Hua, N. Li, M. Chen, F. Teng, Y. Zhu and W. Yao, *J. Mol. Catal. A: Chem.*, 2014, **393**, 302-308.
32. M. Brunel-Laügt, A. Durif and J. Guitel, *J. Solid State Chem.*, 1978, **25**, 39-47.
33. E. M. Walitzi, *Mineral. Petrol.*, 1963, **8**, 614-624.
34. X. Meng, K. Lin, X. Yang, Z. Sun, D. Jiang and F.-S. Xiao, *J. Catal.*, 2003, **218**, 460-464.
35. S. Meng, D. Li, M. Sun, W. Li, J. Wang, J. Chen, X. Fu and G. Xiao, *Catal. Commun.*, 2011, **12**, 972-975.
36. T. Yan, J. Long, X. Shi, D. Wang, Z. Li and X. Wang, *Environ. Sci. Technol.,* 2010, **44**, 1380-1385.